Acta Crystallographica Section D
Biological Crystallography
ISSN 0907-4449

The structure of the BIR3 domain of cIAP1 in complex with the N-terminal peptides of SMAC and caspase-9

Raviraj Kulathila,[a] Brian Vash,[a] David Sage,[a] Susan Cornell-Kennon,[a] Kirk Wright,[a] James Koehn,[a] Travis Stams,[a] Kirk Clark[a] and Allen Price[b]*

[a]Novartis Institutes for Biomedical Research Inc., USA, and [b]Emmanuel College, Boston, USA

Correspondence e-mail: priceal@emmanuel.edu

Received 27 May 2008
Accepted 21 November 2008

PDB References: cIAP1-BIR3, complex with N-terminal peptide from caspase-9, 3d9t; complex with N-terminal peptide from SMAC, 3d9u.

The inhibitor of apoptosis protein (IAP) family of molecules inhibit apoptosis through the suppression of caspase activity. It is known that the XIAP protein regulates both caspase-3 and caspase-9 through direct protein–protein interactions. Specifically, the BIR3 domain of XIAP binds to caspase-9 *via* a 'hotspot' interaction in which the N-terminal residues of caspase-9 bind in a shallow groove on the surface of XIAP. This interaction is regulated *via* SMAC, the N-terminus of which binds in the same groove, thus displacing caspase-9. The mechanism of suppression of apoptosis by cIAP1 is less clear. The structure of the BIR3 domain of cIAP1 (cIAP1-BIR3) in complex with N-terminal peptides from both SMAC and caspase-9 has been determined. The binding constants of these peptides to cIAP1-BIR3 have also been determined using the surface plasmon resonance technique. The structures show that the peptides interact with cIAP1 in the same way that they interact with XIAP: both peptides bind in a similar shallow groove in the BIR3 surface, anchored at the N-terminus by a charge-stabilized hydrogen bond. The binding data show that the SMAC and caspase-9 peptides bind with comparable affinities (85 and 48 n*M*, respectively).

1. Introduction

Because of its extreme consequences, programmed cell death, also known as apoptosis, must be tightly regulated. Both the logic and the structural mechanisms underlying the regulation of this process are areas of current research. An important set of proteins which suppress the apoptotic signal are the IAP (inhibitor of apoptosis protein) family. Although some members of this family are known to repress apoptosis through the inhibition of caspases (Shi, 2004), the functions of all the members are not known. These genes (numbering eight in the human genome) are composed of one to three N-terminal BIR (baculoviral repeat) domains, plus accessory C-terminal domains such as RING, CARD and UBC domains.

The most studied of the IAPs is XIAP (X-linked IAP), which contains three BIR domains and a single C-terminal RING domain. The BIR1 and BIR2 domains are responsible for inhibiting the effector caspases caspase-3 and caspase-7 by competitive inhibition: a linker region between the two domains binds to the active site of the caspases (Shiozaki & Shi, 2004). The BIR3 domain is responsible for inhibiting the initiator caspase caspase-9 by forming a protein–protein complex with the caspase and holding it in an inactive conformation (Shiozaki & Shi, 2004). The BIR3–caspase-9 interaction is regulated by SMAC (also known as DIABLO), a pro-

death signaling protein released from the mitochondria during apoptotic signal transduction. Once activated by cleavage of an N-terminal domain, SMAC releases caspase-9 from the inactive BIR3–caspase-9 complex by direct competition for binding to the BIR3 domain (Liu *et al.*, 2000; Wu *et al.*, 2000). The N-terminal tetrapeptide of the activated SMAC is sufficient to inhibit XIAP–caspase-9 binding *in vitro* (Shi, 2004). Crystal structures have shown that the N-termini of the activated caspase-9 and the activated SMAC bind to the same shallow groove on the surface of XIAP-BIR3.

The IAP-family members cIAP1 and cIAP2 also contain three BIR domains in addition to a CARD and RING domain. Recent experiments have shown that cIAP1 and cIAP2 bind to caspases (Eckelman & Salvesen, 2006) and that the BIR3 domain of cIAP1 is necessary and sufficient for caspase-9 binding. Although it binds, the data do not show inhibition of caspase activity and therefore the biological role of this binding, if any, is unknown. Further work has shown that the BIR3 domain of cIAP1 is required for the ubiquitination of SMAC by cIAP1 (Samuel *et al.*, 2006). cIAP1 contains E3 ligase activity in its RING domain and the data imply that the BIR3 domain is necessary for the recruitment of SMAC to cIAP1 for ubiquitination.

The IAP family contains attractive targets for the development of anticancer therapeutics (Schimmer, 2004). Small-molecule SMAC mimetics (Bockbrader *et al.*, 2005) and antagonists of XIAP (Oost *et al.*, 2004) have shown activity against human cancer cell lines. In addition, synthetic SMAC/DIABLO peptides have been shown to bind both XIAP and cIAP1 *in situ* and to enhance the activity of chemotherapeutic compounds in some cancer cell lines (Arnt *et al.*, 2002).

In order to help elucidate the molecular mechanisms of cIAP1 activity and to explore the possibility of targeting cIAP1 activity with small molecules, we have determined the crystal structures of the BIR3 domain of cIAP1 in complex with N-terminal hexapeptides of the activated (cleaved) forms of both SMAC and caspase-9. We have also measured the binding of these peptides to both cIAP1-BIR3 and XIAP-BIR3 using the surface plasmon resonance technique. Our data show that cIAP1-BIR3 binds these peptides in a manner analogous to the binding of these peptides in XIAP-BIR3. This work also supports the view that the cIAP1-BIR3 protein can be effectively targeted by molecular therapeutics.

2. Materials and methods

2.1. Cloning, expression and purification of protein for SPR

All plasmid vectors employed in the cloning phase were propagated in the TOP10 *Escherichia coli* strain (Invitrogen, Carlsbad, California, USA) in SOC medium (Invitrogen) containing 100 µg ml^{-1} carbenicillin (Teknova, Hollister, California, USA). LB Agar Carbenicillin plates (100 µg ml^{-1}) were purchased from Teknova. Platinum Taq (Hi Fidelity) DNA polymerase and Champion pET151 Directional TOPO Expression Kit were purchased from Invitrogen. DNA-sequence analysis was performed by Agencourt Biosciences, Beverly, Massachusetts, USA. Primers were purchased from Integrated DNA Technologies, Coralville, Iowa, USA.

cIAP1-Avi.N and cIAP1-Avi.C constructs and pBirA plasmid (Avidity, Denver, Colorado, USA) were propagated in BL21(DE3)pLysS (Invitrogen) for protein expression. LB growth medium was purchased from Invitrogen. Chloramphenicol antibiotic and LB Agar Carbenicillin and Chloramphenicol plates (50 and 34 µg ml^{-1}, respectively) were purchased from Teknova. Biotin, IPTG, Trizma base, NaCl, glycerol, imidazole, 2-mercaptoethanol, NP40 and EDTA were all purchased from Sigma–Aldrich, St Louis, Missouri, USA. Complete protease-inhibitor tablets were purchased from Roche Diagnostics, Indianapolis, Indiana, USA. Ni–NTA agarose was purchased from Qiagen, Valencia, California, USA.

cIAP1 BIR3-domain protein containing an NH_2-terminal AviTag was generated by TOPO cloning constructs into the pET151-D/TOPO vector following the manufacturer's instructions. The cDNA encoding human cIAP1 was used as a template for first-round PCR amplification of the cIAP1 BIR3 domain (amino acids 262–364) using the appropriate primers. The PCR products were cloned into the pET151-D/TOPO vector using the Champion pET151 Directional TOPO Expression Kit, transformed into chemically competent TOP10 strain *E. coli* and grown on LB Agar Carbenicillin plates for ∼16 h at 310 K. Randomly selected colonies were screened by colony PCR. Clones yielding PCR products comparable in size to those predicted from the respective input DNA sequences were validated by bidirectional DNA-sequence analyses.

Validated N-terminal AviTagged cIAP1 constructs were co-transformed with the biotin ligase-expressing plasmid pBirA into chemically competent BL21(DE3)pLysS and then grown on LB Agar Carbenicillin/Chloramphenicol plates for ∼16 h at 310 K. Randomly selected colonies were screened for expression of AviTagged proteins in pilot experiments (the induction conditions are described below) and the best candidates were chosen for scale-up. Candidate single BL21(DE3)pLysS colonies containing cIAP1+pBirA were each grown in LB cultures supplemented with 50 µg ml^{-1} carbenicillin, 34 µg ml^{-1} chloramphenicol and 10 µ*M* biotin at 310 K to an OD_{600} of 0.6–0.7. The cells were then induced with 0.5 m*M* IPTG for 3.5 h and centrifuged at 5000*g* for 5 min. The resulting cell pellet was lysed in buffer *A* (50 m*M* Tris pH 8.0, 500 m*M* NaCl, 5% glycerol, 20 m*M* imidazole, 1 m*M* β-mercaptoethanol) supplemented with 1% NP40 and Complete protease-inhibitor mix (Roche) and sonicated for 1 min on ice. The resulting lysate was centrifuged at 277 K for 5 min at 10 000*g* and the supernatant was applied for 1 h onto a nickel-chelating (Ni–NTA) column pre-equilibrated in buffer *A*. The column was washed extensively with buffer *A* and the protein was eluted at 300 K over an 18 h period with buffer *A* supplemented with 100 U constitutively active TEV protease for the cell paste from an initial 4 l culture. The resulting protein was dialyzed in buffer *B* (50 m*M* Tris pH 8.0, 150 m*M* NaCl, 10% glycerol, 1 m*M* EDTA and 1 m*M* DTT) and concentrated. The yield was 5–10 mg protein with a purity of

greater than 98% by SDS–PAGE for each clone from an initial 4 l culture.

2.2. SPR biosensor measurement

All surface plasmon resonance measurements were performed at 298 K using a Biacore T100 instrument. The immobilization buffer and running buffer was 10 m*M* HEPES, 150 m*M* NaCl, 0.005% P20 pH 7.4 containing 2.5 m*M* DTT and 2% DMSO. Biotinylated IAP protein was immobilized at densities of 2000–2500 response units on the streptavidin sensor-chip surface. To collect kinetic binding data, concentration series of SMAC or caspase-9 peptide in running buffer were injected over the ligand and reference flow cells at a flow rate of 60 µl min^{-1}. During each injection, the ligand was allowed to associate with the immobilized IAP protein (analyte) for 60 s and the ligand–analyte complex was allowed to dissociate for 1000 s. All response data were double referenced and data were fitted globally to a 1:1 interaction model using Biacore T100 Evaluation Software (v.1.1).

2.3. Cloning, expression and purification of protein for crystallization

DNA corresponding to residues 250–352 of the BIR3 domain of cIAP1 was amplified by PCR and cloned into pNAT40 expression vector (N-terminal 6×His followed by a PreScission cleavage site). The 6×His-cIAP1 expression vector was transformed into *E. coli* BL21(DE3)Star cells and subsequently grown overnight at 310 K to saturation in ZYP-0.8G media. This culture served as a starter for further fermentation and induction in ZYP-5052 auto-induction media according to the method of Studier (2005). The cells were grown to saturation (~24–30 h at 291 K), collected by centrifugation and frozen at 193 K. The frozen cell pellets were resuspended and lysed using an EmulsiFlex-C5 High-Pressure Homogenizer in a fivefold excess (*w*/*v*) of lysis buffer consisting of 25 m*M* HEPES, 25 m*M* MES, 100 m*M* NaCl, 5 m*M* TCEP, protease-inhibitor tablets (Boehringer-Mannheim), 100 µ*M* PMSF, 10 µg ml^{-1} DNase I pH 7.0. The soluble lysate obtained by centrifugation (100 000*g* for 60 min) was diluted in a 1:1 ratio with 25 m*M* MES, 25 m*M* HEPES pH 7 to lower the ionic strength. Cation-exchange chromatography was performed using a POROS HS 50 column (PerSeptive Biosystems) equilibrated with dilution buffer at a flow rate of 25 ml min^{-1}. Bound protein was eluted at pH 7 using a 0–500 m*M* NaCl gradient. The fractions containing cIAP1 (300–400 m*M* NaCl) were pooled, concentrated and buffer-exchanged into 25 m*M* MES, 25 m*M* HEPES, 100 m*M* NaCl, 1 m*M* EDTA, 2 m*M* DTT pH 7.0. The fusion protein was cleaved overnight at 277 K with PreScission Protease and then passed over a 5 ml HisTrap column (GE Healthcare) to remove the 6×His tag. The untagged protein was concentrated and purified to its final form by size-exclusion chromatography on a 500 ml Superdex 75 HiLoad column (Amersham Biotech) equilibrated with 50 m*M* HEPES, 100 m*M* NaCl, 1 m*M* TCEP pH 8.0.

Table 1
Data-collection and refinement statistics.

Values in parentheses are for the highest resolution shell.

	cIAP1-BIR3–caspase-9	cIAP1-BIR3–SMAC
Data collection		
Space group	$P2_12_12_1$	$P6_122$
Unit-cell parameters (Å)	a = 30.3, b = 68.4, c = 122.4	a = 63.0, b = 63.0, c = 115.3
Resolution (Å)	1.5 (1.50–1.55)	2.3 (2.30–2.38)
R_{merge}	0.052 (0.257)	0.191 (0.876)
$I/\sigma(I)$	35.4 (5.5)	20.7 (4.0)
Completeness (%)	99.7 (98.6)	97.7 (96.8)
Redundancy	6.4 (5.6)	15.7 (15.6)
Refinement		
No. of reflections	40966	6193
R_{work}/R_{free}	0.183/0.205	0.201/0.256
Number of atoms		
Overall	1909	877
Protein	1559	749
Ligand/ion	82	43
Water	268	85
Mean B factor (Å^2)	19.6	31.3
R.m.s.d.		
Bond lengths (Å)	0.014	0.006
Bond angles (°)	1.3	1.0

2.4. Structure determination

The hexapeptides AVPIAQ (SMAC) and ATPFQE (caspase-9) were purchased from Invitrogen Corp. The protein–peptide complexes were cocrystallized using hanging-drop vapor diffusion. A stock of each peptide was prepared (1–3 mg ml^{-1}) and added to the protein solution (5 mg ml^{-1}) so that the final molar ratio of protein:peptide was 1:1.5. The complex was then concentrated to 11.0 mg ml^{-1} in 20 m*M* HEPES pH 8.0, 0.1 m*M* NaCl and incubated for 30 min on ice. Diffraction-quality crystals were grown using vapor diffusion in a drop made by mixing 1.5 µl protein solution and 1.5 µl well solution. In both cases, the crystals grew to full size within 3–5 d. The ATPFQE cocrystals with the best diffraction grew in 2.7–3.1 *M* sodium formate, 0.1 *M* Tris pH 7.5–8.5, 10% glycerol at 293 K. These crystals were cryoprotected in 4.0 *M* NaF, 0.1 *M* Tris pH 7.5–8.5, 20% glycerol and then flash-frozen in liquid nitrogen. The AVPIAQ cocrystals grew in 0.1 *M* bis-Tris pH 6.5, 0.2 *M* $MgCl_2$, 22% PEG 3350 at 293 K. These crystals were cryoprotected in 0.1 *M* bis-Tris pH 6.5, 0.2 *M* $MgCl_2$, 20% glycerol and then flash-frozen in liquid nitrogen.

Crystals were transferred from mother liquor to a cryoprotectant, mounted in Hampton loops and frozen by plunging them into liquid nitrogen. Data were collected on the IMCA beamline, sector 17, at the Advanced Photon Source, Argonne National Laboratory. All data were processed with *HKL*-2000 (Otwinowski & Minor, 1997). Final data statistics can be found in Table 1. The structure of the cIAP1-BIR3–caspase-9 peptide complex was determined using the molecular-replacement method. The program *Phaser* v.1.3 (Storoni *et al.*, 2004) was used to place a polyserine model created from the XIAP-BIR3 monomer (PDB code 1nw9; Shiozaki *et al.*, 2003). *ARP*/*wARP* (Morris *et al.*, 2003) was used to build the cIAP1-BIR3 sequence into the density.

Cycles of refinement using *CNX* (Brünger *et al.*, 1998) and manual rebuilding using *O* (Jones *et al.*, 1991) and *Coot* (Emsley & Cowtan, 2004) were used to refine the model. Waters were picked with *CNX*. The final statistics of the refinement are shown in Table 1.

The SMAC peptide complex was built in a similar manner, but using the cIAP1-BIR3–caspase-9 peptide complex structure as a search model. A few cycles of manual rebuilding using *CNX* and *Coot* completed the model. The final statistics are given in Table 1.

3. Results

3.1. SPR results

The binding constants of both the caspase-9 peptide (ATPFQE) and the SMAC peptide (AVPIAQ) to cIAP1-BIR3 were measured using the surface plasmon resonance technique. The measured sensograms are shown in Fig. 1. Fits to this data allowed the determination of the equilibrium binding constants. The caspase-9 peptide (ATPFQE) binds to the BIR3 domain of cIAP2 with an affinity of 48 ± 2 n*M*, whereas the SMAC peptide (AVPIAQ) binds with an affinity of 85 ± 8 n*M*.

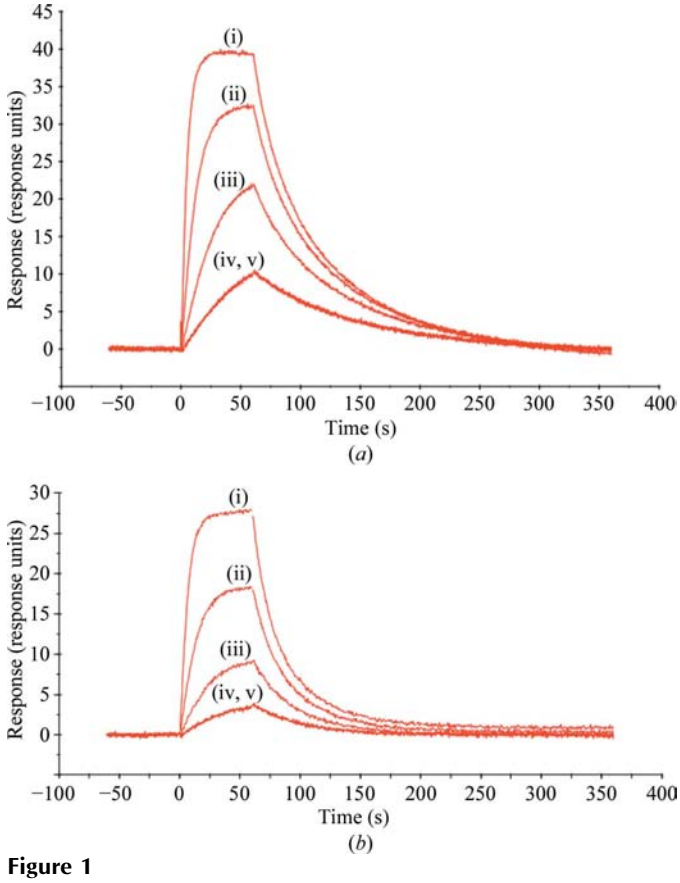

Figure 1
SPR measurement of the binding of the peptides to cIAP1-BIR3. The binding of peptides (analyte) to immobilized CIAP1-BIR3 (ligand) was measured using a Biacore T100 instrument. The sensograms represent serial dilutions of peptides: (i) 370 n*M*, (ii) 123 n*M*, (iii) 41 n*M*, (iv) 14 n*M* and (v) 14 n*M* (duplicate), respectively. Peptides were diluted in HBS-P+ buffer containing 2.5 m*M* DTT and injected in separate cycles at a flow rate of 100 µl min^{-1}. Note that the first 60 s of each trace (at times before t = 0) show the baseline before peptide injection. Also, the trace is truncated at 360 s and does not show the entire dissociation phase. (*a*) Binding of caspase-9 peptide (ATPFQE). (*b*) Binding of SMAC peptide (AVPIAQ).

3.2. Evaluation of the crystal structures

The structure of the cIAP1-BIR3–caspase-9 peptide complex was refined to 1.5 Å resolution. The complex crystallized in space group $P2_12_12_1$, with two molecules per asymmetric unit. The first seven N-terminal residues in monomer *A* and the first two N-terminal residues in monomer *B* are not visible in the electron density; they were presumed to be disordered and hence were excluded from the final model. The crystal packing shows a crystal contact near the peptide-binding site in monomer *A*, whereas the binding site of monomer *B* is open to a large solvent channel. Since the monomer *B* binding site is judged to be less influenced by crystal contacts and hence is expected to reproduce more faithfully what occurs in the solution state, it is this monomer that will be shown in all figures in the paper. The two peptides and their respective binding sites do not superimpose exactly owing to this difference (the r.m.s.d. of all atoms between the two binding sites is 0.39 Å excluding the peptide). A single zinc ion is present per monomer. The final *R* factors (R_{work} = 0.183, R_{free} = 0.205) show excellent agreement between the model and the data. Stereochemical analyses of the structure with *PROCHECK* (Laskowski *et al.*, 1993) and *WHATCHECK* (Hooft *et al.*, 1996) show good stereochemistry. The final refinement statistics are shown in Table 1.

The structure of the cIAP1-BIR3–SMAC peptide complex was refined to 2.3 Å resolution. The complex crystallized in the hexagonal space group $P6_122$, with one molecule per asymmetric unit. The first four N-terminal residues and the last C-terminal residue are not visible in the electron density; they were presumed to be disordered and hence were excluded from the final model. A single zinc ion was found to bind to the protein. The final structure for this complex shows good agreement with data (R_{work} = 0.201, R_{free} = 0.256) and good stereochemistry as determined by *PROCHECK* and *WHATCHECK*. The final statistics for this structure are shown in Table 1.

3.3. The structure of cIAP1-BIR3

The cIAP1-BIR3 complexes are shown in Fig. 2. A comparison of the two crystal structures shows the conformations of the protein to be the same, with minor differences owing to side-chain conformations located at crystal contacts. As shown in Fig. 2, the cIAP1-BIR3 domain adopts an α/β-fold which supports a central Cys-Cys-His-Cys zinc-finger motif. The structure can be divided into halves: the N-terminal portion, residues 252–308, forms the $\alpha_1\alpha_2\beta_1\beta_2\beta_3$ motif and contains the first two residues (Cys300–Cys303) of the zinc finger. The C-terminal $\alpha_3\alpha_4\alpha_5$ motif, residues 253–346, contains the final two residues of the zinc finger (His320–Cys327). The structural zinc ion bridges the two parts of the molecule. The peptide-binding site (in both complexes) is

located in a shallow cleft at the C-terminus of strand β3 at the boundary between the two halves of the molecule.

3.4. Protein–ligand interactions

The specific interactions between the caspase-9 peptide and cIAP1-BIR3 are shown in Fig. 3(*a*). A central interaction involves hydrogen bonds between the amide N atom and the carbonyl O atom of caspase-9 Thr317 and the backbone amide and carbonyl of cIAP1 Arg308. These interactions continue the antiparallel β-sheet core of the BIR3 domain, with the peptide playing the role of a fourth strand. The N-terminus of the peptide is anchored by a charge-stabilized hydrogen bond to the side-chain carboxyl group of cIAP1 Asp314. In contrast, the C-terminal end of the peptide veers away from cIAP1-BIR3 strand β3 and a water molecule is inserted between the carbonyl O atom of caspase-9 Phe319 and the amide N atom of cIAP1 Gly306. Thus, the antiparallel hydrogen-bonding pattern between protein and ligand is broken, allowing the peptide to place the side chain of caspase-9 Phe319 into the shallow groove formed between cIAP1 residues Arg308, Glu297, Gly306 and Lys299. Other notable interactions are the hydrogen bonds between the Ala316 carbonyl O atom of the peptide and the cIAP1 Trp323 side chain. The caspase-9 Ala316 side chain is nestled in a hydrophobic pocket formed by cIAP1 Trp310 and Leu307. The central proline moiety of the peptide covers the hydrophobic patch created by cIAP1 residues Trp323, Phe324 and Leu307. The C-terminal residues caspase-9 Gln320 and Glu321 do not interact with cIAP1-BIR3. The electron density indicates that the side chains and terminal carboxyl groups are slightly disordered in the crystal structure.

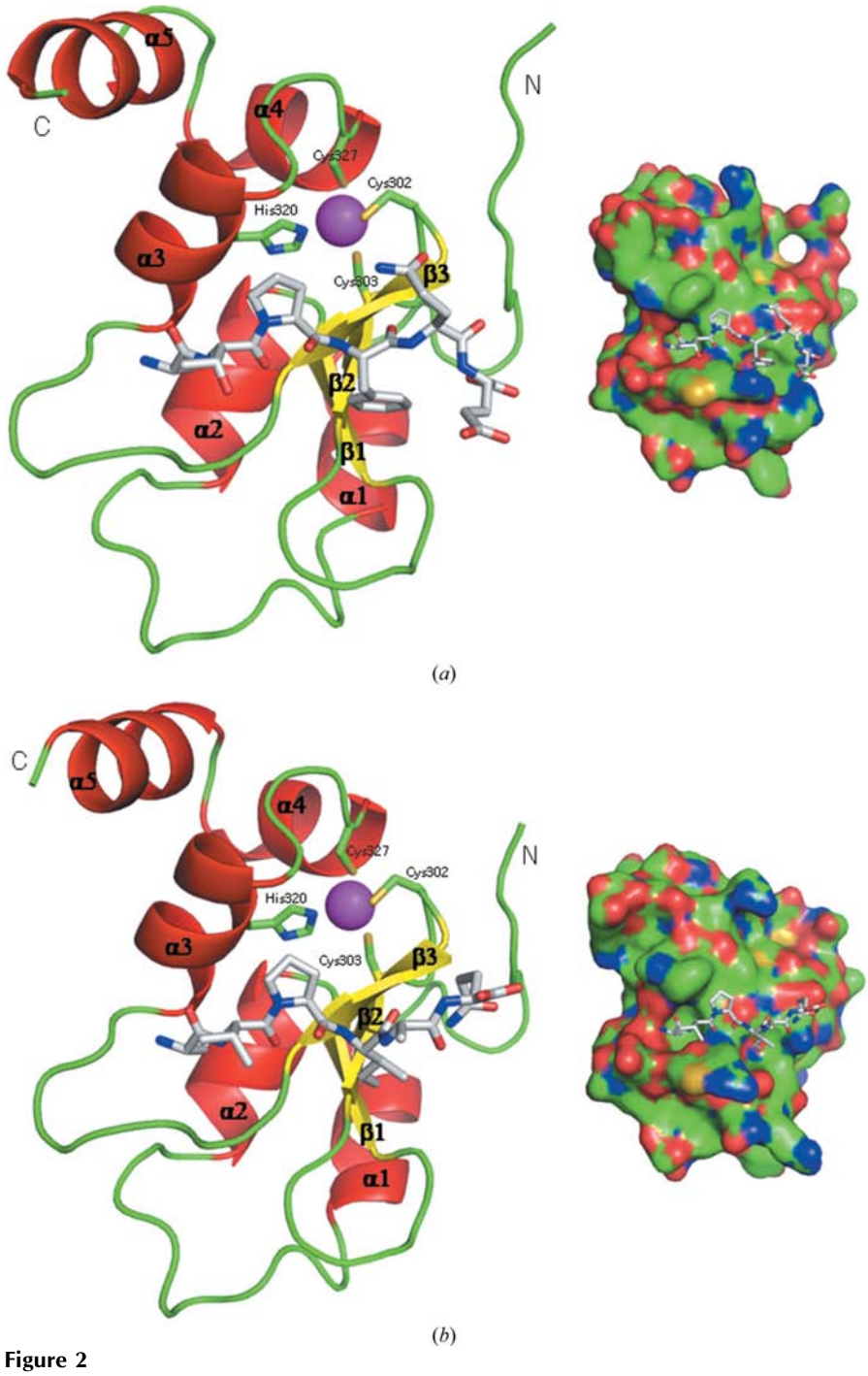

Figure 2
Structures of the cIAP1-BIR3–peptide complexes. The cIAP1-BIR3 domain is shown in ribbon representation (α-helices in red, β-strands in yellow and other regions in green). The conventional naming of the secondary structures is shown. The peptides are shown in stick representation. The residues involved in zinc coordination are shown explicitly. The purple sphere represents the zinc ion. The inset in each panel shows a surface representation of the complexes with the protein. The surface is colored to represent the identity of the atoms at the surface (O, red; N, blue; C, green; S, yellow). (*a*) The cIAP1-BIR3–caspase-9 peptide complex. (*b*) The cIAP1-BIR3–SMAC peptide complex.

The interactions between cIAP1-BIR3 and the SMAC peptide are shown in Fig. 3(*b*). The SMAC peptide resides in the same groove as the caspase-9 peptide, forming a continued fourth strand in the antiparallel β-sheet core of the BIR3 domain. The backbone carbonyl O atom and amide N atom of SMAC Val57 form hydrogen bonds to the backbone amide N atom and the carbonyl C atom of cIAP1 Arg308. The N-terminus of the peptide is anchored by a charge-stabilized hydrogen bond between the N-terminal N atom of the peptide and Asp314. The side chain of SMAC Ile59 sits in the pocket formed by the cIAP1 residues Gly306, Lys299, Arg308 and Asp297. Crystal-contact interactions stabilize the conformation of the C-terminus of the SMAC

peptide. SMAC Ala60 sticks out of the pocket, where it is stabilized by a crystal contact with Tyr272 and Asn295 from neighboring cIAP1 molecules. Also, the C-terminal carboxyl group of the SMAC peptide is stabilized by a salt bridge with Arg294 from a symmetry-related molecule.

4. Discussion

4.1. Comparison of SMAC peptide and caspase-9 peptide binding

The binding of the SMAC peptide and the caspase-9 peptide are compared in the overlay shown in Fig. 4 (monomer *B* of the cIAP1-BIR3–caspase-9 peptide complex is shown). The residues in the binding site are in the same conformation, except for a slight difference in the position of the guanidinium group of cIAP1 Arg308. In the SMAC structure, an Asn295 side chain from a symmetry-related cIAP1 molecule is placed between the Arg308 side chain and Ile59 of the peptide. The conformations of the peptides are seen to be very similar for the first four amino acids of the peptides. Phe319 of the caspase-9 peptide overlays with the Ile59 side chain of SMAC. The two C-terminal residues do not overlay. Residues 320 and 321 of the caspase-9 structure appear to be slightly disordered and do not make specific interactions with the protein binding site, whereas in the SMAC structure the C-terminal residues are stabilized by a crystal contact. The similarities in the binding of the two peptides to cIAP1-BIR3 as observed in these crystal structures are consistent with the SPR measurements. The binding affinities measured are within a factor of two [the equilibrium binding constant of the caspase-9 peptide (ATPFQE) is 48 n*M*, whereas that of the SMAC peptide (AVPIAQ) is 85 n*M*].

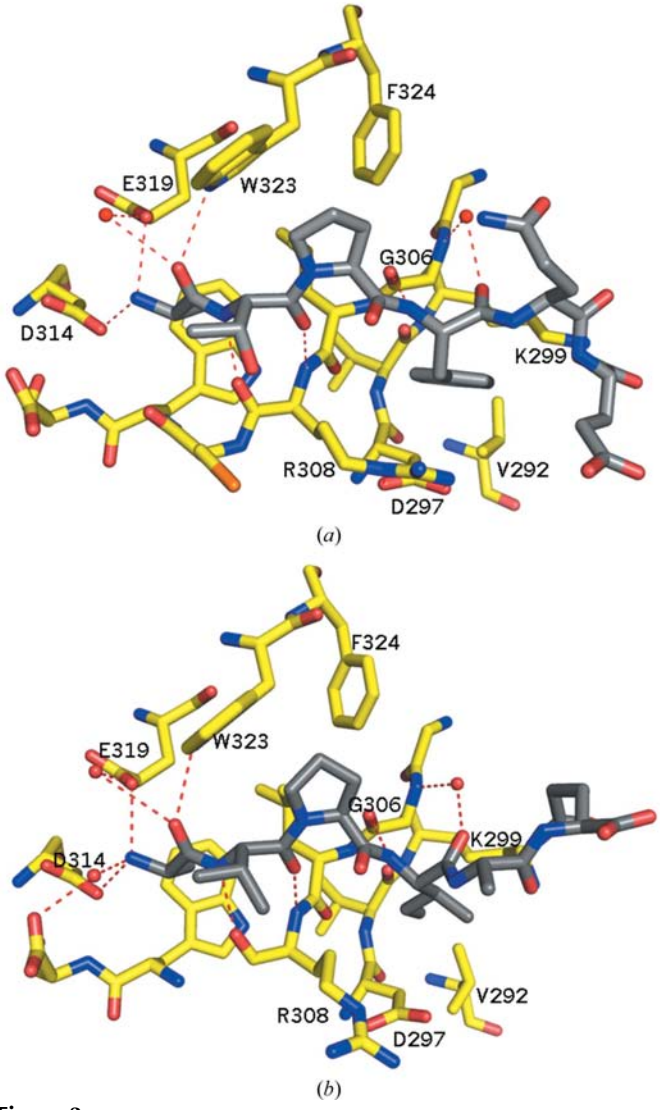

Figure 3
cIAP1-BIR3–peptide interactions. The cIAP1-BIR3 protein is shown with yellow C atoms. The peptides are shown with gray C atoms. Hydrogen bonds are represented by dotted red lines. (*a*) The cIAP1-BIR3–caspase-9 peptide complex. (*b*) The cIAP1-BIR3–SMAC peptide complex.

4.2. Comparison of cIAP1-BIR3 to XIAP-BIR3

The BIR3 domains of cIAP1 and XIAP share a sequence identity of 48% and hence are expected to have similar structures. Fig. 5 shows that this is indeed the case. The folds of the two domains are seen to be the same. The r.m.s.d. of the C^{α} atoms of the two superimposed structures is only 0.75 Å. The peptide-binding sites in the two proteins share many features. As shown in Fig. 6(*a*), the binding site of the cIAP1-BIR3–caspase-9 complex superimposes closely with the peptide-binding site of the XIAP-BIR3–caspase-9 protein–protein complex. Asp314 (Glu314 in XIAP) participates in a charge-

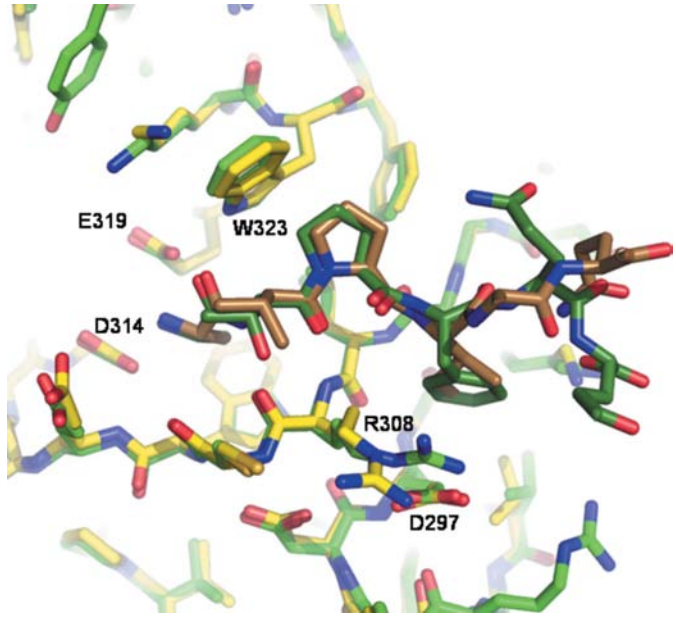

Figure 4
Comparison of the caspase-9 and SMAC peptides from the crystal structures. An overlay of the binding sites from the protein–peptide complexes is shown. In the cIAP1-BIR3–SMAC peptide (sequence AVPIAQ) structure, cIAP1-BIR3 is shown with yellow C atoms and the peptide with brown C atoms. In the cIAP1-BIR3–caspase-9 peptide (sequence ATPFQE) structure, cIAP1-BIR3 is shown with light green C atoms and the peptide with dark green C atoms.

stabilized hydrogen bond to the N-terminal amino group of the peptide. Leu307 and Trp310 (conserved in XIAP) form the hydrophobic pocket for the side chain of the peptide alanine. In XIAP, the shallow hydrophobic pocket which binds the large hydrophobic side chain of the peptide (Phe318 in caspase-9, Ile59 in SMAC) is composed on one side by Gly306 and Lys299 and on the other by the aliphatic portion of the side chain of Lys297. One side of this pocket is conserved (Gly306 and Lys299), but the other side has Lys297 of XIAP replaced by Asp297 in cIAP1. By forming a salt bridge with Arg308, this substitution preserves a hydrophobic binding pocket in cIAP1. The aliphatic portions of these larger residues (Arg308 and Asp297) form a hydrophobic pocket which is deeper in cIAP1 than in XIAP.

4.3. Comparison of the binding of peptides in cIAP1-BIR3 and XIAP-BIR3

There are no published crystal structures of XIAP-BIR3 in complex with either the caspase-9 (ATPFQE) or the SMAC (AVPIAQ) hexapeptides. However, structures are available of the full protein–protein complexes XIAP-BIR3–caspase-9 (PDB code 1nw9; Shiozaki *et al.*, 2003) and XIAP-BIR3–SMAC (PDB code 1g73; Wu *et al.*, 2000). We will compare our structures with these.

Fig. 6(*a*) shows a comparison of the cIAP1-BIR3–caspase-9 peptide complex and the N-terminal peptide-binding site of the XIAP-BIR3–caspase-9 protein–protein complex (PDB code 1nw9). Alternate rotamers of Thr317 and Pro318 are seen in the two structures. Thr317 is seen to have distinct χ_1 values and the pucker of the proline ring is different in the two structures (in XIAP the γ carbon of the pyrrolidine points into the binding site, whereas in cIAP1 it points outwards). These differences could be caused by the different binding sites in XIAP and cIAP1. Near caspase-9 Pro318, the binding site residue 324 is a tyrosine in XIAP while it is a phenylalanine in cIAP1. Likewise, near caspase-9 Thr317, Asp309 of XIAP is replaced by a cysteine in cIAP1. Another possible explanation involves the different environments surrounding the two binding sites. In the cIAP1-peptide structure the hexamer peptide is exposed to a large solvent channel. In the XIAP–caspase-9 complex caspase-9 Pro336 and the carbonyl between Leu335 and Pro336 lie over the two peptide residues Thr317 and Pro318 and may influence their conformation. In XIAP, the carbonyl of Ser333 is hydrogen bonded to the backbone amine of peptide residue Gln320 and is likely to

Figure 5
Overlay of cIAP1-BIR3 and XIAP-BIR3. The C^{α}-atom traces of the proteins are shown. cIAP1-BIR3 is shown in magenta and XIAP-BIR3 in gray. The conformation of cIAP-BIR3 from the caspase-9 peptide complex (this work) is superimposed on the XIAP-BIR3 structure as seen in the protein–protein complex of XIAP-BIR3 and caspase-9 (Shiozaki *et al.*, 2003). The coordinated zinc ion is shown in magenta.

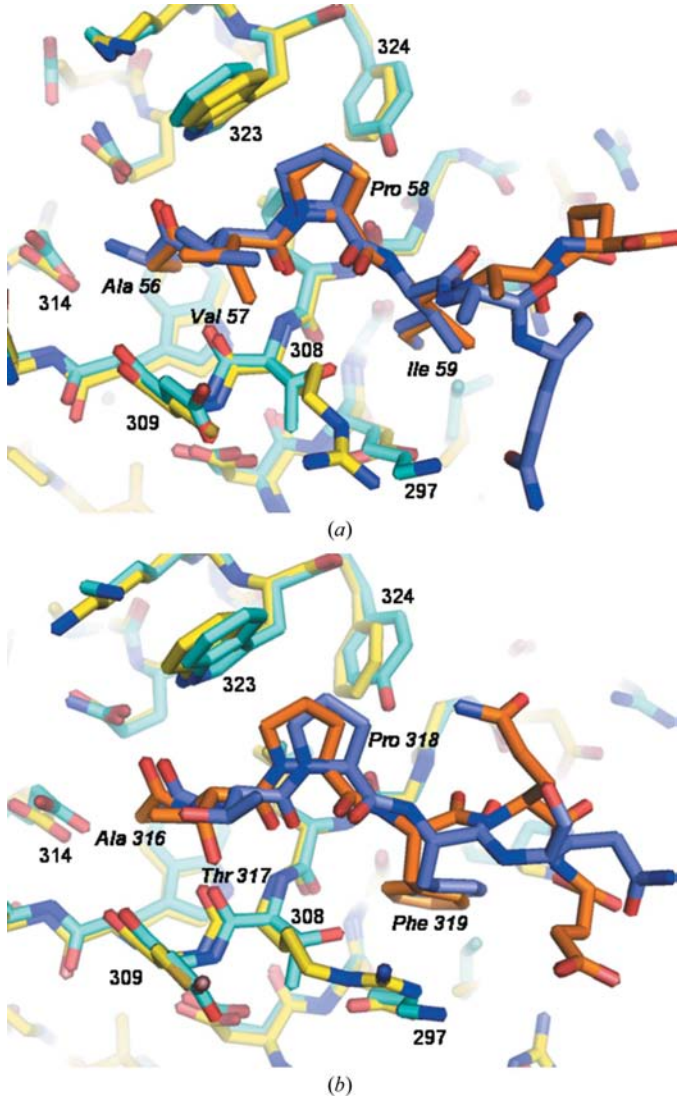

Figure 6
Comparison of peptide binding in cIAP1-BIR3 and XIAP-BIR3. Overlays of the peptide binding in cIAP1-BIR3 and XIAP-BIR3 are shown. The cIAP1-BIR3 structure is shown with yellow C atoms and its bound peptide with orange C atoms; the XIAP-BIR3 structure is shown with cyan C atoms and its bound peptide with purple C atoms. The XIAP-BIR3 peptide structures are taken from the protein–protein complexes (the rest of the SMAC and caspase-9 proteins is not shown). (*a*) Overlay of SMAC peptide binding in cIAP1-BIR3 and XIAP-BIR3. (*b*) Overlay of caspase-9 peptide binding in cIAP1-BIR3 and XIAP-BIR3.

influence its conformation. The conformations of the peptides in the cIAP1 and XIAP structures diverge for residues 320 and 321. This divergence is accounted for by the different environments surrounding the peptides in the two structures and is not a consequence of specific interactions within the binding sites. Hence, although most of the interactions are determined by the N-terminal peptide sequence, the presence of the rest of the caspase-9 protein influences the details.

A comparison of the cIAP1-BIR3–SMAC peptide complex (present study) with the XIAP-BIR3–SMAC protein–protein complex (PDB code 1g73) is shown in Fig. 6(*b*). Again, the binding modes are similar and the peptides from the two structures superimpose except for a few minor differences. Slight differences in the conformations of SMAC Val57 could be a consequence of the substitution of Asp309 in XIAP by cysteine. Note that this difference parallels what was observed in the caspase-9 complexes. Alternatively, it could result from the presence of crystal contacts in the cIAP1 structure. Tyr272 from a symmetry-related cIAP1-BIR3 molecule makes a crystal contact with the SMAC Pro58 carbonyl group in the peptide structure, whereas this residue is free from crystal contacts in the previously published protein–protein complex. In addition, differences in the two binding modes are seen for SMAC residues 61 and 62. This is likely to be a consequence of the crystal contact that the carboxy-terminus of the hexapeptide in the cIAP1-BIR3 complex makes with a neighboring protein (a salt bridge with Arg294 from a neighboring cIAP1 molecule; see §3).

4.4. Relation of the protein–peptide complexes to the protein–protein complexes

How do the protein–peptide interactions we report compare with the binding of the peptides in the context of the full cIAP1-BIR3–SMAC or cIAP1-BIR3–caspase-9 protein–protein complexes? We cannot make a direct comparison as there is no published structure of cIAP1-BIR3 in complex with either caspase-9 or SMAC. Some light can be shed on this issue by an examination of the structure of the XIAP-BIR3–AVPF tetrapeptide complex (PDB code 2opz; Wist *et al.*, 2007), which shows the conformation of the bound peptide to be similar to that of the first four residues in both the full XIAP-BIR3–SMAC complex and the XIAP-BIR3–caspase-9 complex. Note that the AVPF sequence is not identical to either the SMAC N-terminal tetrapeptide (AVPI) or the caspase-9 N-terminal tetrapeptide (ATPF). However, the AVPF sequence has similarity to both the SMAC and caspase-9 peptides. The only difference is in the second amino acid, which points out of the binding site, and the fourth residue, which makes a hydrophobic interaction. These observations demonstrate that in XIAP-BIR3 at least the conformation of the first four peptides is determined by the direct interactions between the peptide and the binding pocket and is not greatly influenced by the presence of the rest of either SMAC or caspase-9. Without the complete cIAP1-BIR3–caspase-9 and cIAP1-BIR3–SMAC protein–protein complexes, we cannot prove a similar statement for cIAP1-BIR3. However, the observations of what occurs in XIAP-BIR3 suggest that our cIAP1-BIR3–peptide complexes represent faithfully the conformations of the peptides that occur in the complete cIAP1-BIR3 protein–protein complexes.

5. Concluding remarks

We have determined the first crystal structures of the BIR3 domain of cIAP1 and have measured the binding constants of peptides using SPR. The structures show molecular details of the interactions of cIAP1 and the N-terminal peptides from SMAC and caspase-9. These structures and our binding data show that the binding modes of the two peptides to cIAP1-BIR3 are similar in specific interactions and in affinity. A comparison of our results with XIAP structures shows that the interactions between the peptides and cIAP1 are similar to the interactions of these peptides with XIAP. Differences observed in the binding mode of the hexapeptides are restricted to the fifth and sixth amino acids, which are influenced by the environments in the structures. Previous results have shown that the first four amino acids of these peptides are sufficient for binding (Arnt *et al.*, 2002). Our results are consistent with these data, showing that the conserved specific interactions are confined to these residues.

It has been shown that SMAC prevents XIAP from inhibiting caspase-9 by direct competition with caspase-9 for the same binding surface on XIAP (Liu *et al.*, 2000; Wu *et al.*, 2000). It is also known that binding of the N-terminal peptide of SMAC is necessary for the protein–protein interaction: mutagenesis of these required residues prevents complex formation (Srinivasula *et al.*, 2000; Chai *et al.*, 2000). However, the exact details of the functional relationship between cIAP1 and SMAC are unknown. It has been shown that cIAP1 leads to the degradation of SMAC by direct physical interaction and subsequent ubiquitination of SMAC (Samuel *et al.*, 2006). Our work provides evidence that the protein–protein interaction between cIAP1 and SMAC is organized around the same hotspot present in the XIAP–SMAC interactions; specifically, the binding of the N-terminal tetrapeptide of SMAC.

Experiments show that cIAP1 binds to caspase-9 and that the BIR3 domain is necessary for this interaction. However, the evidence does not support the idea that cIAP1 inhibits caspase-9 using the same mechanism as XIAP, as cIAP1 by itself does not inhibit caspase-9 activity (Eckelman & Salvesen, 2006).

Our work elucidates the mechanism by which cIAP1 binds to the N-terminal peptide of caspase-9. The structure of the cIAP1-BIR3–caspase-9 N-terminal peptide presented in this report shows the binding of the peptide in the same tetrapeptide-binding 'hotspot' present in XIAP. Further experiments are necessary before the biological role, if any, of this interaction can be elucidated.

Use of the IMCA-CAT beamline 17-ID (or 17-BM) at the Advanced Photon Source was supported by the companies of the Industrial Macromolecular Crystallography Association

through a contract with the Center for Advanced Radiation Sources at the University of Chicago.

References

Arnt, C. R., Chiorean, M. V., Heldebrant, M. P., Gores, G. J. & Kaufmann, S. H. (2002). *J. Biol. Chem.* **277**, 44236–44243.

Bockbrader, K. M., Tan, M. & Sun, Y. (2005). *Oncogene*, **24**, 7381–7388.

Brünger, A. T., Adams, P. D., Clore, G. M., DeLano, W. L., Gros, P., Grosse-Kunstleve, R. W., Jiang, J.-S., Kuszewski, J., Nilges, M., Pannu, N. S., Read, R. J., Rice, L. M., Simonson, T. & Warren, G. L. (1998). *Acta Cryst.* D**54**, 905–921.

Chai, J., Du, C., Wu, J.-W., Kyin, S., Wang, X. & Shi, Y. (2000). *Nature (London)*, **406**, 855–862.

Eckelman, B. P. & Salvesen, G. S. (2006). *J. Biol. Chem.* **281**, 3254–3260.

Emsley, P. & Cowtan, K. (2004). *Acta Cryst.* D**60**, 2126–2132.

Hooft, R. W. W., Vriend, G., Sander, C. & Abola, E. E. (1996). *Nature (London)*, **381**, 272.

Jones, T. A., Zou, J.-Y., Cowan, S. W. & Kjeldgaard, M. (1991). *Acta Cryst.* A**47**, 110–119.

Laskowski, R. A., MacArthur, M. W., Moss, D. S. & Thornton, J. M. (1993). *J. Appl. Cryst.* **26**, 283–291.

Liu, Z., Sun, C., Olejniczak, E. T., Meadows, R. P., Betz, S. F., Oost, T., Herrmann, J., Wu, J. C. & Fesik, S. W. (2000). *Nature (London)*, **408**, 1004–1008.

Morris, R. J., Perrakis, A. & Lamzin, V. S. (2003). *Methods Enzymol.* **374**, 229–244.

Oost, T. K. *et al.* (2004). *J. Med. Chem.* **47**, 4417–4426.

Otwinowski, Z. & Minor, W. (1997). *Methods Enzymol.* **276**, 307–326.

Samuel, T., Welsh, K., Lober, T., Togo, S. H., Zapata, J. M. & Reed, J. C. (2006). *J. Biol. Chem.* **281**, 1080–1090.

Schimmer, A. D. (2004). *Cancer Res.* **64**, 7183–7190.

Shi, Y. (2004). *Protein Sci.* **13**, 1979–1987.

Shiozaki, E. N., Chai, J., Rigotti, D. J., Riedl, S. J., Li, P., Srinivasula, S. M., Alnemri, E. S., Fairman, R. & Shi, Y. (2003). *Mol. Cell*, **11**, 519–527.

Shiozaki, E. N. & Shi, Y. (2004). *Trends Biol. Sci.* **29**, 486–494.

Srinivasula, S. M., Datta, P., Fan, X.-J., Fernandes-Alnemri, T., Huang, Z. & Alnemri, E. S. (2000). *J. Biol. Chem.* **275**, 36152–36157.

Storoni, L. C., McCoy, A. J. & Read, R. J. (2004). *Acta Cryst.* D**60**, 432–438.

Studier, W. F. (2005). *Protein Expr. Purif.* **41**, 207–234.

Wist, A. D., Gu, L., Riedl, S. J., Shi, Y. & McLendon, G. L. (2007). *Bioorg. Med. Chem.* **15**, 2935–2943.

Wu, G., Chai, J., Suber, T. L., Wu, J.-W., Du, C., Wang, X. & Shi, Y. (2000). *Nature (London)*, **408**, 1008–1012.